JJMIE

Volume 20, Number 3, September 2026
ISSN 1995-6665
Pages 385– 403
https://doi.org/10.59038/jjmie/200306
Editor-in-Chief: Prof. Faris M. AL-Oqla

Jordan Journal of Mechanical and Industrial Engineering

Cr_2O_3-Enhanced Al-4%Cu Alloys: Unveiling Microstructural Refinement and Superior Mechanical Performance

Cynthia C. Nwaeju-Okechukwu[a,b*], Ekerete U. Affiah[b] , Silas. O Okuma[a], M. Saravana Kumar[c,d] , Francis O. Edoziuno[b,e]

[a]Department of Mechanical Engineering, Nigeria Maritime University, Okerenkoko, P.M.B. 1005, Warri, Delta State, Nigeria.
[b]Department of Metallurgical and Materials Engineering, Nnamdi Azikiwe University, P.M.B. 5025 Awka, Nigeria.
[c]Graduate Institute of Manufacturing Technology, National Taipei University of Technology, Taipei 10608,Taiwan.
[d]Department of Mechanical Engineering, Saveetha School of Engineering, Saveetha Institute of Medical and Technical Sciences (SIMATS), Chennai, Tamil Nadu 602105, India.
[e]Department of Mechanical, Aerospace & Acoustical Engineering, University of Hartford, 200 Bloomfield Avenue, West Hartford, CT 06117, USA.

Received 2 Oct 2025 Accepted 7 Feb 2026

Abstract

Enhancing the mechanical performance of Al–Cu alloys through cost-effective alloying particle strategies remains a significant challenge in materials engineering. This study investigates the influence of Cr_2O_3 particle additions on the properties and microstructure of Al-4%Cu alloys by varying the Cr_2O_3 content from 0.75 to 2.25 wt% in 0.25 wt% intervals, representing a compositional approach not previously reported. Mechanical properties were evaluated using tensile, hardness, and impact tests, while microstructural evolution was examined using optical microscopy and scanning electron microscopy. The results were compared between Cr_2O_3-free alloys and Cr_2O_3-reinforced alloys. The findings reveal that the addition of Cr_2O_3 particles promotes significant grain refinement, contributing to notable improvements in the alloy's mechanical performance. The tensile properties (ultimate tensile strength, yield strength, and ductility) of the Al-4%Cu alloy increased markedly with increasing Cr_2O_3 content, showing improvements of 53.03%, 42.14%, and 38% within the 1.50–2.25 wt% range compared to the unreinforced alloy. However, hardness and impact energy decreased with increasing Cr_2O_3 content, with optimum values observed at 0.75 wt%. This work establishes a systematic and economically viable route for enhancing the mechanical properties of Al–Cu alloys through composition-optimized Cr_2O_3 particle additions, offering new insights into the design and development of high-performance lightweight materials.

Keywords: Al/Cu/Cr2O3, grain refinement, microstructure, mechanical properties, chemical composition.

1. Introduction

Aluminium and its alloys exhibit a unique combination of mechanical, thermal, and electrical properties, making them essential in various engineering applications. These materials are characterized by a high strength-to-weight ratio, excellent elasticity, superior malleability, and ease of machinability. Additionally, they offer outstanding corrosion resistance and exceptional thermal and electrical conductivity. A key advantage of aluminium alloys is their ability to undergo multiple recycling cycles without degradation in their inherent metallurgical properties, reinforcing their significance as sustainable engineering materials [1–3]. These advantages establish aluminium alloys as advanced structural materials, particularly for next-generation applications in the transportation and aerospace sectors [4]. Płonka et al. [1] emphasized the importance of evaluating the impact of variations in the composition of primary alloying elements when developing new aluminium alloys, as these changes significantly affect the material's properties and suitability for specific application. In recent years, the demand for lightweight, high-strength materials has increased significantly, particularly in the construction and transportation sectors. This trend has driven extensive research into modifying and enhancing the properties of aluminium alloys to meet evolving engineering demands. The use of lightweight materials has emerged as a key research focus in the 21st century, emphasizing the growing need to modify and enhance the properties of aluminium alloys to meet specific application requirements [5,6]. Aluminium alloys, particularly the 6xxx and 2xxx series, are widely utilized for lightweight structural applications. However, due to the stringent performance requirements in the aviation and transportation industries, 2xxx series alloys are generally preferred for these demanding application [1,7].

* Corresponding author e-mail: cynthianwaeju@gmail.com.

Aluminium-copper alloys achieve moderate strength through the formation of the intermetallic compound $Al_2Cu(\theta)$, which precipitates as a non-coherent phase during slow cooling to ambient temperature [8]. Studies have consistently shown that copper addition improves both strength and toughness. Its solubility enables effective heat treatment, alloying, and the maximization of mechanical properties [9,10]. With these advantages, single-phase Al-Cu alloys face limitations in achieving the optimal balance of high strength and ductility required for modern industrial applications [9]. Engineering components with diverse mechanical and technological properties are continuously being developed, with key influencing factors such as alloying element and its composition, plastic deformation parameters, and heat treatment conditions [9,11–13]. To address this, researchers have explored micro-alloying techniques to introduce secondary phase precipitates that refine the alloy structure and improve its mechanical properties. Adding oxide and carbide particles into aluminium alloys has been widely explored to enhance the properties. For instance, the addition of Al_2O_3 oxide particles has been reported to improve the mechanical performance of Al6061 alloys [14]. Likewise, nano-sized SiC particles have been utilized to strengthen Al–Cu alloy as reported by [15]. CuO additions has been reported to significantly enhance the electrical conductivity and tensile properties of aluminium alloy [16].

Various alloy processing techniques, such as thermomechanical processing, annealing, and aging treatments have been shown as effective methods for enhancing the strength, hardness, and electrical conductivity of aluminium based alloys [17]. The composition and casting conditions of an alloy significantly influence its mechanical properties, as they control the development of intermetallic phases [18,19]. Previous research has highlighted the benefits of adding single alloying elements to aluminium alloys, which in turn leads to grain refinement and improved mechanical strength. Chen et al. [20] showed La additions to Al-Cu-Mn alloys promote a higher density of θ phases and grain refinement, enhancing mechanical properties. Additionally, the study by Meng and Wang [21] on the effect of vanadium addition in Al-Cu-Mn alloys revealed that vanadium promotes the precipitation of the θ (Al_2Cu) phase along the grain boundaries, facilitating the growth of the θ-phase within the α(Al) matrix while simultaneously suppressing the formation of the $\theta(Al_{20}Cu_2Mn_3)$ phase. Su et al. [12] in their study on the influence of Mg on the microstructure and mechanical properties of Al-Cu-Mn alloys observed that the addition of Mg contributed to significant grain refinement. This refinement was attributed to the transformation of the primary strengthening phase from the θ-(Al_2Cu) phase to the (Al_2CuMg) phase, indicating that Mg plays a crucial role in modifying the phase composition and enhancing the alloy's mechanical performance. Płonka et al. [1] investigated the influence of copper content on the structure and properties of aluminium alloys, modifying the copper content to 2.5%, 3.5%, and 4.5%. Their findings indicated that the alloys based on the 6xxx series exhibited improved properties with copper addition, including a finer grain structure. Wang et al. [22] also explored the effects of copper content and lanthanum on the properties of aluminium-copper alloys, specifically the Al-La alloy. By adding 0.5 wt.% of La and varying the copper content, they observed that grain refinement occurred up to a certain copper concentration. Zheng et al.[23] carried a study on the impact of La on the microstructure and properties of an Al-Cu-Si alloy. Their findings showed that La had diverse effects on enhancing the strength of the Al alloy. Pinning and grain refinement mechanisms contributed to the enhanced overall properties [23,24]. Ding et al. [25] reported that the addition of Ce element refines the grains of Al-Cu-Li alloy. When the Ce content is below 0.1%, the ultimate strength of the alloy increases with the rising Ce content. Although much has been written about the impact of individual single alloying elements such as Mg, Si, Ca, La, and Ce on the properties of Al-Cu alloys, there remains a notable gap in research regarding the effects of Cr and Cr_2O_3 addition on both the microstructure and mechanical performance of these Al-Cu alloys.

Grain refinement is a critical process in aluminium alloy production, as it significantly impacts the mechanical properties and microstructural characteristics of the final product. The use of grain refiners to inoculate the molten alloy has been identified as an effective technique for refining the as-cast microstructure and mitigating the occurrence of hot tearing in Al-Cu-Mg alloys. Various alloying elements, such as Mg, Si, Ca, La, and Ce, have been extensively studied for their grain-refining effects. [26,27]. Additionally, chromium (Cr) has been shown to influence grain refinement in aluminium alloys by modifying the nucleation and growth processes [28,29]. The use of Cr_2O_3, in particular, offers advantages due to its high thermal stability and ability to act as a nucleating agent for grain refinement, as demonstrated in similar alloy systems [30]. Chromium oxide (Cr_2O_3) is a refractory material known for its complete solubility in aluminium oxides, forming $(Al_{1-x}Cr_x)_2O_3$ at high temperatures without eutectic formation across the composition range [31]. This unique solubility enhances its compatibility with aluminium alloys, providing excellent corrosion resistance and thermal stability. Furthermore, copper, as an alloying element, has been reported to increase the electrochemical potential difference between the matrix and precipitates, promoting pitting corrosion [51]. The addition of Cr_2O_3 could potentially mitigate these adverse effects by combining passive film formation, microstructural refinement, and electrochemical stabilization, improving the overall corrosion resistance of Al-Cu alloys in aggressive chloride-rich conditions [49]. According to Birks et al. (2006), the $(Al,Cr)_2O_3$ solid solution exhibits superior resistance to high-temperature oxidation and sulfidation compared to pure Al_2O_3 [50]. Despite these established benefits of $(Al,Cr)_2O_3$ solid solutions in high-temperature environments, there is a notable lack of systematic research on the direct addition of as-cast Al-4%Cu alloys with varying concentrations of Cr_2O_3. Specifically, the literature has not yet established how incremental additions (0.25 wt% intervals) of this refractory oxide influence the competitive growth between α--Al matrix and θ-phase ($CuAl_2$) during solidification. Moreover, the critical transition point for the changeover of Cr2O3 from an ideal grain refiner to an undesirable inclusion affecting impact toughness has not yet been reported. The current research work fills this research void by incorporating a comprehensive linking between Cr2O3 content, grain refinement, and associated trade-offs in mechanical properties. The chromium has been shown to influence nucleation and growth behaviour, but there is a lack of systematic understanding of how Cr_2O_3 particles interact with the Al–Cu matrix to modify microstructure and mechanical performance, especially in Al-4%Cu alloys under as-cast conditions. Therefore, the present research work will look into the influence of Cr_2O_3 variation on the microstructure and mechanical properties of Al-4%Cu alloy in the as-cast condition. It tends to identify an optimum composition of Cr_2O_3 that would improve the performance of the alloy while maintaining its structural integrity

2. Materials and Experimental procedures

2.1. Materials Process

The alloy ingots produced in this work were prepared using an oil-fired crucible furnace under an N_2 atmosphere. The presence of an N_2 atmosphere is to prevent the alloy from oxidising during the melting process [3]. Analytical-grade aluminium wires, copper wires (98.99% purity), and Cr_2O_3 powder (99.99% purity) were used as raw materials for the fabrication of Al–4%Cu–xCr_2O_3 alloys. The designed compositions of the developed Al–4%Cu–xCr_2O_3 alloys are presented in Table 1. Melting was carried out in a graphite crucible with a capacity of 10 kg. Aluminium with a chemical composition exceeding 90% was first charged into the furnace and heated to its melting temperature of 660 °C. Subsequently, a weighed copper wire, wrapped in aluminium foil and slightly preheated, was introduced into the molten aluminium and held for 8 min to ensure complete dissolution of copper in the aluminium melt. The melt was then stirred at 200 rpm for 6 min to promote uniform dispersion and homogeneity. After intermittent stirring to further ensure homogeneity, the molten metal was cast into a preheated permanent steel mould with dimensions of 45 × 55 × 155 mm³ to produce the control sample. After complete melting of the aluminium and copper wires, Cr_2O_3 of particle size of 45 µm were added to the molten metal at varying concentrations ranging from 0.75 to 2.25 wt%, in intervals of 0.25 wt%. This addition range was selected to optimize the mechanical properties of the $(Al,Cr)_2O_3$ solid solution and enhance scale adhesion. Following adequate stirring to ensure homogenization, the composite melt was poured into a preheated steel mould. This procedure was followed as described in [22,25,33,34]. Eight samples were produced and coded as presented in Table 1. The chemical composition of the cast Al-4%Cu alloy without Cr_2O_3 powder was determined after casting using a Spark Emission Spectrometer (SES) of Model W6, and the result is presented in Table 2.

2.2. Characterization

The characterization of the cast Al-4%Cu-xCr_2O_3 alloys focused on evaluating their microstructure and mechanical properties. The structural analysis emphasized the dispersion of intermetallic particles within the microstructure and the assessment of grain size.

Table 1. Chemical Compositions of the designed alloy (wt. %) before casting

Alloy designation	Elemental composition (wt. %)		
	Cr_2O_3	**Cu**	**Al**
A0	0	4.0	Bal
A1	0.75	4.0	Bal
A2	1.0	4.0	Bal
A3	1.25	4.0	Bal
A4	1.5	4.0	Bal
A5	1.75	4.0	Bal
A6	2.0	4.0	Bal
A7	2.25	4.0	Bal

Table 2. Chemical Compositions of the produced Al-4%Cu alloy (wt.%)

Mg	Fe	Ti	Si	Mn	C	B	N	Cu	Al
0.12	0.16	0.06	0.04	0.01	0.03	0.01	0.21	4.09	Bal

For the microstructural analysis, an optical metallurgical microscope (OM-L2003A) and a scanning electron microscope (PHENON-ProX) were utilized. Prior to this process, the samples were cut to a mounting size and cold mounted in a thermosetting material. The mounted samples were initially ground with different grit sizes of SiC paper (600, 800, 1200, 1600, 2000 µm), polished automatically using aluminium oxide powder to achieve a mirror-like surface, followed by etching. The etching process, which exposes the polished surface for microstructural examination, was performed in aqueous hydrochloric acid for 25 seconds, then rinsed in water and dried with a METASER specimen dryer. The optical micrographs were produce at magnification x400. The three-dimensional view (3D) of the obtained microstructure of the cast alloys, as well as the average grain size and distribution, were determined using the linear intercept method with Image J software. Image J is an analytical software that provides quantitative information on various parameters of the microstructure, such as phase fraction percentage, particle size, shape parameter index, etc [35]. The procedures for determining these parameters on the microstructure of the cast Al-4% Cu-xCr_2O_3 alloys are as described in Ref. [36,37]

The mechanical properties evaluated in this study include ultimate tensile strength, yield strength, ductility (percentage elongation), hardness, and impact resistance. Tensile tests were performed on specimens machined to the specified dimensions illustrated in Fig. 1, utilizing an Instron universal testing machine (Model 3369) under ambient conditions. The tensile specimens followed the ASTM B557M standard and were machined with dimensions of 100 mm sample length, 65 mm gauge length, 8 mm gauge diameter, and 10 mm grip diameter, while maintaining a strain rate of 10^{-3} s^{-1} throughout the testing. Hardness measurements were conducted using a TESTOR HT 1 Otto Wolpert-Werke Rockwell hardness testing apparatus. The hardness evaluation involved a 15 kgf indentation force and a 100 kgf load for scratch testing over a 30-second duration. Measurements were taken at three distinct locations on each specimen to mitigate the influence of alloy segregation, with the mean values recorded. A standard conversion chart was used to convert the measured Rockwell hardness values into Brinell hardness values. A Charpy impact machine (Model MT-004) was used to measure energy absorption capability. V-notched samples, as shown in Fig. 2, were machined to a standard size of 55 mm in length and 10 mm × 10 mm cross-section according to the ASTM E23-18 standard to determine the impact strength of the cast alloys. A deep notch with a radius of 0.25 mm at an angle of 45° was obtained on a standard size of 55 mm in length and 10 mm x 10 mm in diameter sample to determine the impact strength of the developed alloys. An average of at least three specimen results was taken for all the mechanical properties results.

3. Results and Discussions

3.1. Optical microscopy and grain analysis

The morphological characteristics such as grain size and shape, as well as the size of the constituent phase, were evaluated using optical microscopy. The distinctive optical microstructure of a cast Al-4%Cu alloys with different contents of Cr_2O_3 are shown in Fig 3. The microstructures of the alloy are different as the content of Cr_2O_3 increases. Fig. 3a illustrates the microstructure of the Al-4%Cu alloy, which serves as the base alloy for this study. The microstructure shows relatively coarse grains and non-uniform distribution of Cu-rich intermetallic. This indicates limited grain refinement and weaker particle pinning, which typically results in lower strength and hardness [38]. The microstructural evolution of the Al-4%Cu alloy with the incorporation of Cr_2O_3 is depicted in Figs. 3(b-h). A noticeable grain refinement effect was observed, as the coarse grains present in the base alloy (Al-4%Cu) progressively diminish with increasing Cr_2O_3 content, indicating its role in grain modification and structural homogenization. This suggests that Cr_2O_3 particles function as potent grain refiners in aluminium alloys, contributing to improved microstructural integrity and mechanical performance [28,38]. Cr_2O_3 addition overpass the formation of α $+CuAl_2$ that usually formed in the matrix of Al-Cu alloy.Cr_2O_3 particles act as effective nucleation sites during solidification, restricting grain growth. With different Cr_2O_3 contents added to the base alloy, the grain sizes decreased and the grain boundary became clear and uniform. The grain refinement effect on the microstructure becomes more evident as the Cr_2O_3 particle content increases. Specifically, as the Cr_2O_3 concentration rises from 1.75 wt% to 2.25 wt% (Figs. 3f-h), a noticeable reduction in grain size is observed, accompanied by a more refined microstructure and the formation of thicker grain boundaries, indicating enhanced structural integrity.

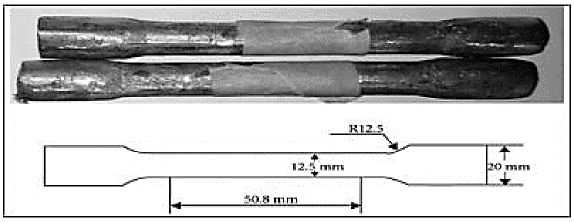

Figure 1. Tensile test Specimen

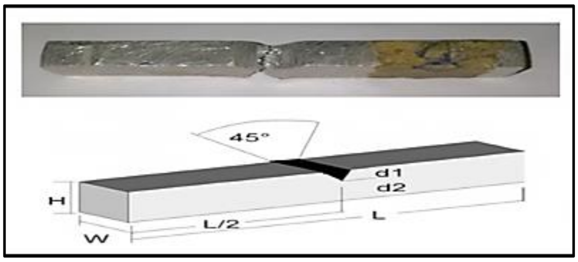

Figure.2 Impact strength test specimen

The size statistics of the secondary dendrite arm spacing (SDAS) and the average grain size of the alloy were analysed, and the results are summarized in Table 3. When Al-4%Cu is alloyed with Cr_2O_3, a significant change in grain size is observed. When different content of Cr_2O_3 were added from 0 to 2.25 wt%, the corresponding SDAS of Al-4%-xCr_2O_3 alloys values are 26.34±0.43 µm, 16.42±1.11 µm, 13.25±1.73 µm, 17.03±1. 39 µm, 14.17 ± 1.48µm 15.18±2.02 µm, 14.24± 1.23 µm, and 12.82±0.47 µm, respectively. The SDAS of the base alloy is relatively large, measuring 26.34±0.43 µm. Comparing with the base alloy, it could be observed that the addition of Cr_2O_3 results in a decrease in the SDAS of the alloy. The SDAS of the α-Al decreases by 37.66%, 49.69%, 35.35%, 42.37%, 45.94%, and 51.33%, respectively, with the addition of Cr_2O_3 from 0.75 wt% to 2.25 wt%.

Fig 4 shows the grain size distribution of the alloy with and without Cr_2O_3 particles. Image processing was performed using ImageJ software, and the average grain size was measured. The optical microscopy (OM) images were utilized to estimate the average grain size of Cr_2O_3-reinforced particles. The histogram demonstrates that the size distribution follows a Gaussian fit based on a log-normal function, with the standard deviation values presented in Table 2 corresponding to the best fit for the experimental data. As depicted in Fig 4, the grain size distribution aligns well with the Gaussian fit, represented by the solid line, confirming the accuracy of the statistical analysis [39,40]. From this distribution gauge fit, it can be observed that the grain data is primarily composed of smaller values, except for the base alloy fit, where the higher grain data is identified (Fig. 4a). The fraction of the average grain size of the Al-4%Cu alloy with 0 wt%, 0.75 wt%, 1.0 wt%, 1.25 wt%, 1.5 wt%, 1.75 wt%, 2.0 wt%, and 2.2 wt5% Cr_2O_3 content were presented in Table 3. It could be observed that there is a significant change in the grain size of the Al-4%Cu alloy by alloying with Cr_2O_3. The average grain size gradually decreases with increasing Cr_2O_3 content, highlighting Cr_2O_3's ability to impede grain boundary migration and inhibiting grain growth [28,36,38]. The fraction of the Al-4%Cu alloy is higher than the alloys with Cr_2O_3 contents. The addition of Cr_2O_3 particles reduces the grain size of the alloy. However, when the Cr_2O_3 contents increases from 0.75 to 2.25 wt%, no significant changes in grain size are observed. The variations in grain sizes within the alloys could be attributed to the fact that the particles are composed of several crystallites, leading to these changes [41]. According to related literatures [28,38], the appropriate addition of chromium in aluminium alloys promotes recrystallization, whereas an excessive amount of chromium retards the recrystallization process. This could as a result, explain the variations seen in the grain size data.

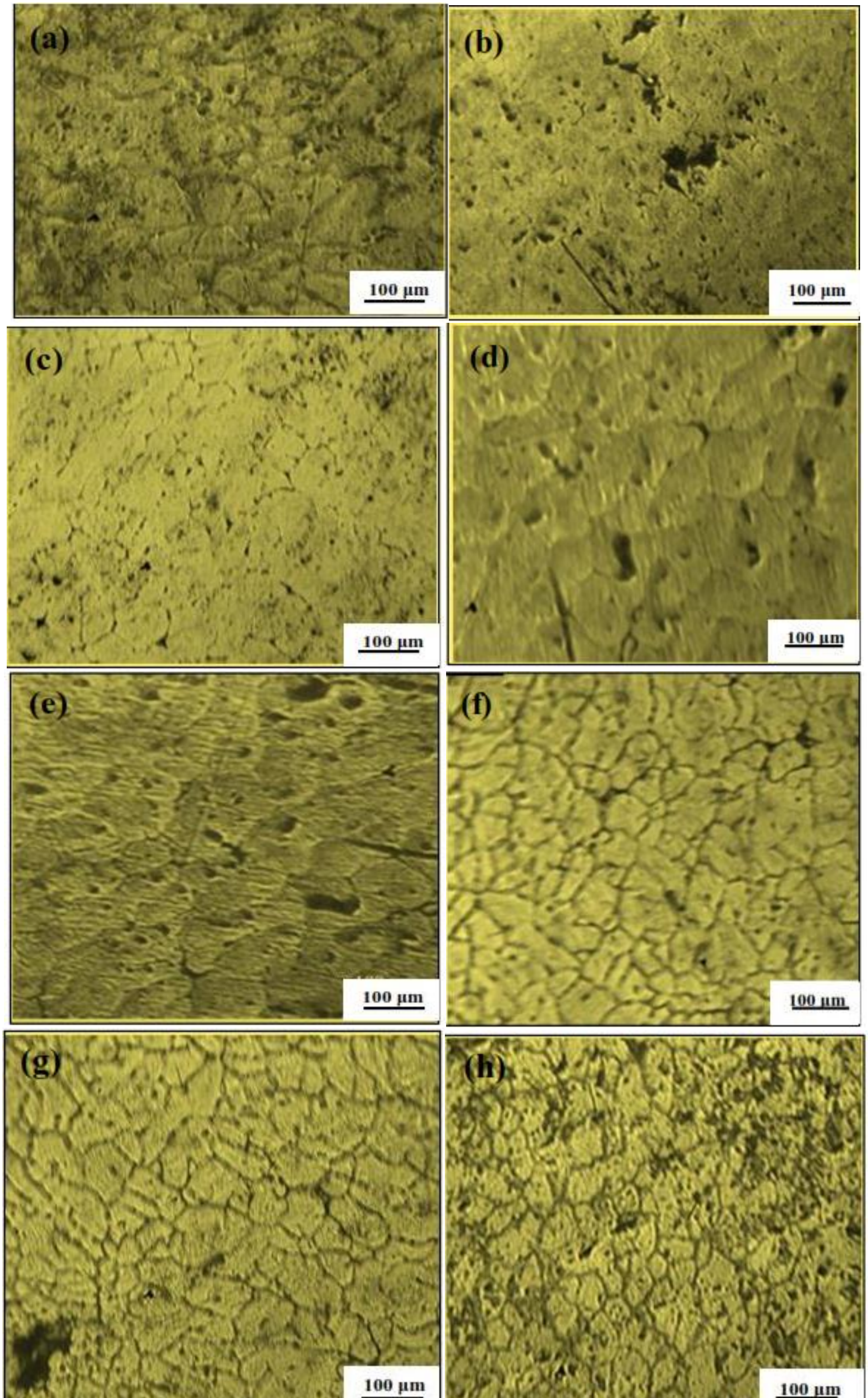

Figure 3. Optical micrographs of as-cast Al-4%Cu alloy with different Cr_2O_3 contents at x400 (a) 0, (b) 0.75, (c) 1.0, (d) 1.25 (e) 1.5 (f) 1.75 (g) 2.0 (h) 2.25 wt%

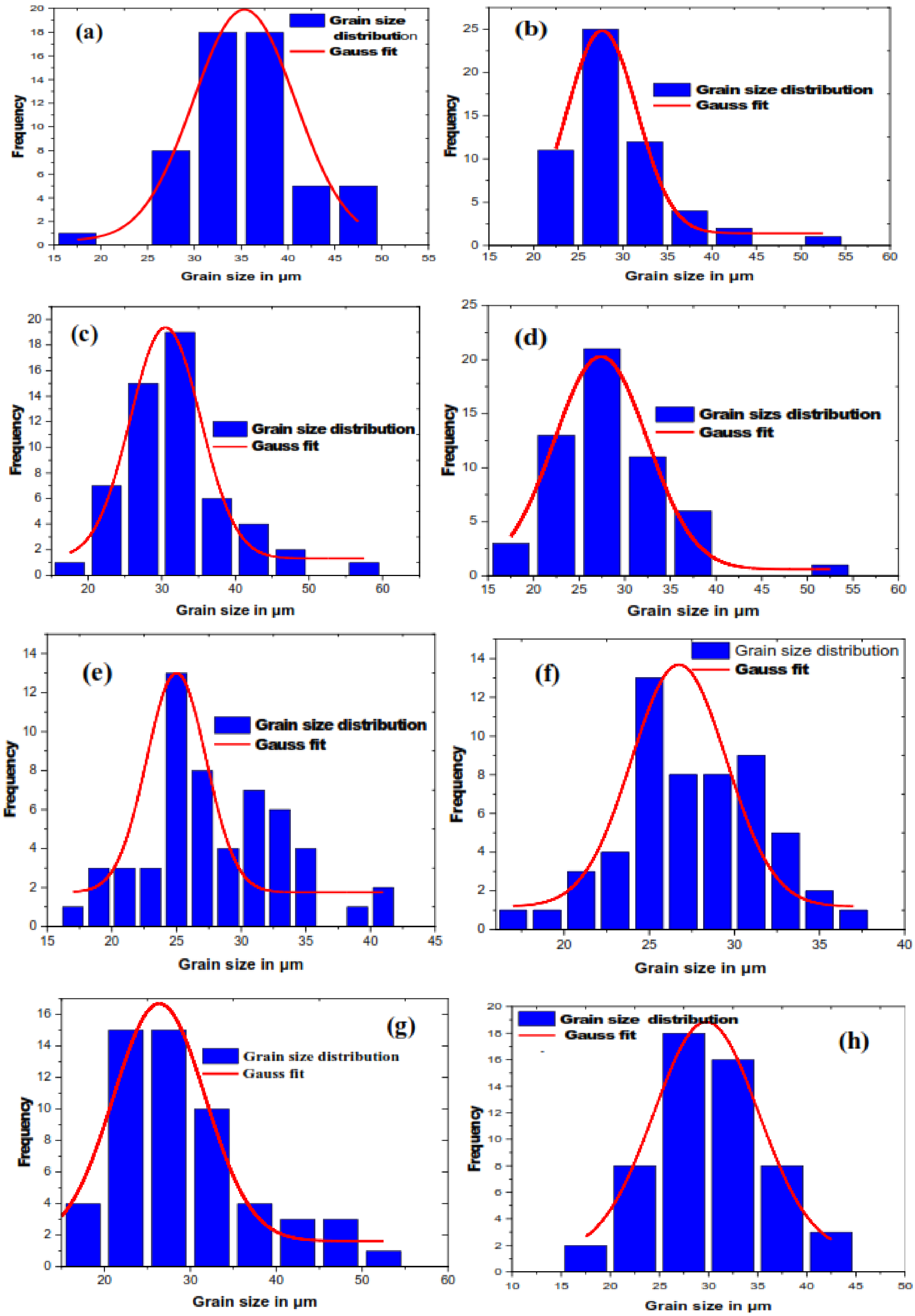

Figure 4. Grain size distribution of Al-4% Cu-xCr_2O_3 alloy from optical images (a) 0, (b) 0.75 (c) 1.0 (d) 1.25 (e) 1.5 (f) 1.75 (g) 2.0 (h) 2.25 wt%

Fig. 5 presents the optical image misorientation map of the alloy which was carried out using imageJ software. As shown in Fig 5a, the orientation map of the base alloy reveals large, coarse, elongated grains. The mapping indicates small lamellar spacing, suggesting limited recrystallization during the alloying process. The grain refinement resulting from the addition of Cr_2O_3 is attributed to the function of intermetallic compounds, which facilitate grain recrystallization during alloy processing. Image analysis based on optical micrographs proves suitable for obtaining accurate grain size distribution information [25,38,41]. The Al-4%Cu-xCr_2O_3 alloys display a greater presence of recrystallized structures compared to the base alloy. The misorientation maps in Figs. 5(b-h) reveal the evolution of various elongated microstructural grains, suggesting Cr_2O_3 addition alters the phase composition of the alloy based on its varying content. Also, the structural parameter alteration in the alloy which include grain size, grain diameter, grain twin, and grain misorientation was as a result of the particle addition. The statistical analysis of recrystallized grains from image misorientation mapping is shown in Fig. 6. The chart indicates that the mean grain diameter gradually decreases with the addition of Cr_2O_3 from 0.75 to 1.5 wt%, but minimal changes are observed from 1.75 to 2.25 wt%, as the mean grain diameter increases slightly from 216.69 µm to 226.06 µm. The variations in the mean grain diameter could be due to the appropriate amount of Cr_2O_3 induces recrystallization, whereas excessive Cr_2O_3 may cause changes during recrystallization process [38].

Table 3. Results of optical image grain analysis of the Al-4%-xCr_2O_3 alloys

Cr_2O_3 contents (wt.%)	Count	Average particle Size After Thresholding (µm)	Std. Dev (µm)	Total Area (µm)	%Area	SDAS Size Distribution (µm)
0	149	35.09	±5.93	1047.37	47.34	26.34 ± 0.43
0.75	105	28.89	±5.49	675.440	27.74	16.42 ± 1.11
1.0	154	31.29	± 7.48	499.79	20.008	13.25 ± 1.73
1.25	100	27.86	±5.78	1702.89	48.63	17.03 ± 1. 39
1.5	115	26.96	±5.4	782.230	42.41	14.17 ± 1.48
1.75	120	27.61	±5.40	782.230	42.42	15.18 ± 2.02
2.0	134	27. 91	±7.78	728.58	45.34	14.24 ±1.23
2.25	151	29.02	±6.11	2191.32	37.66	12.82 ± 0.47

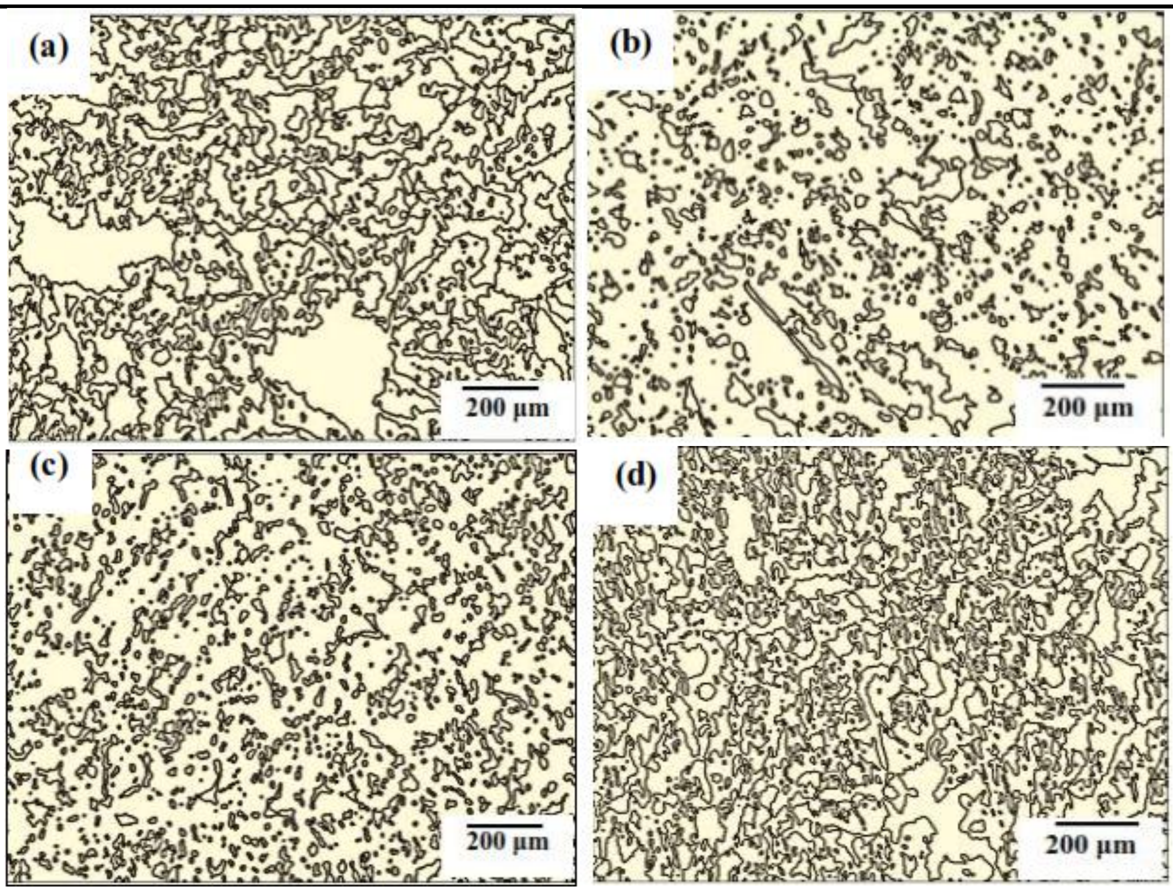

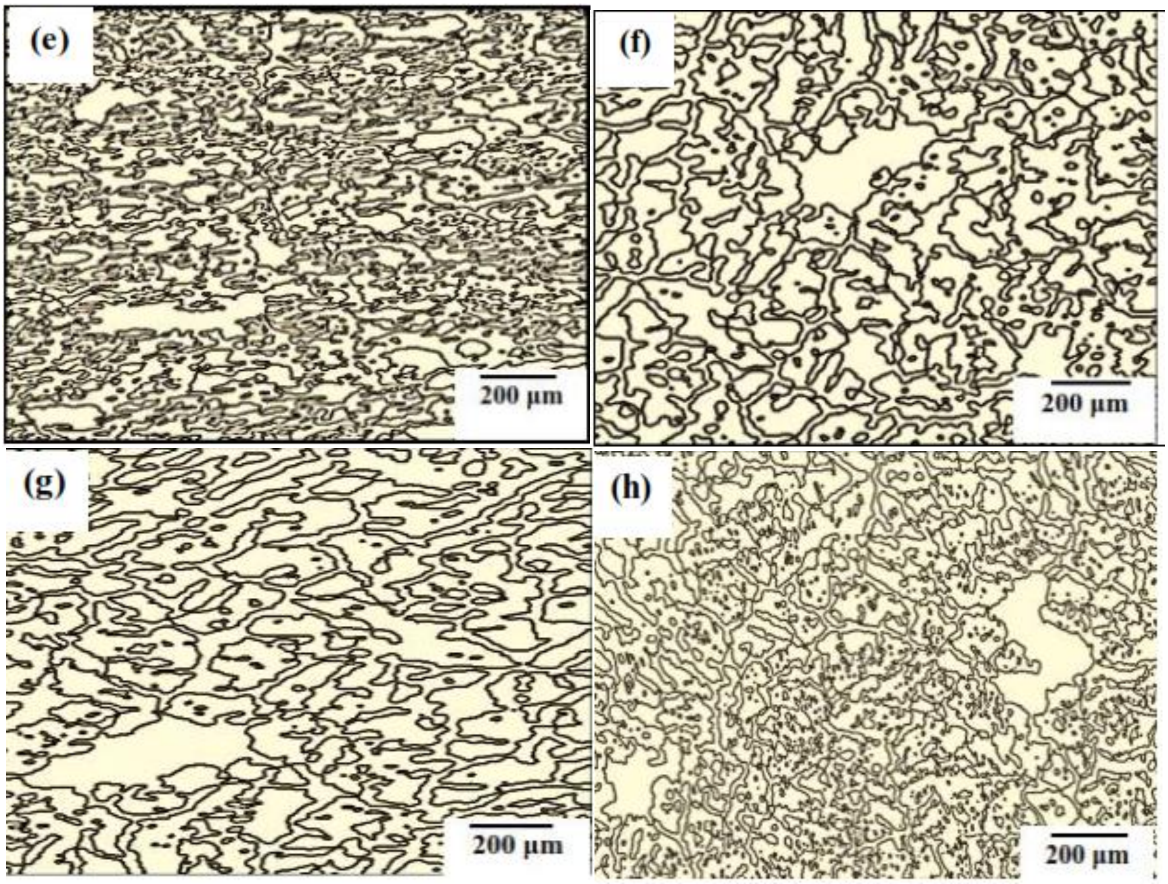

Figure 5. Optical image misorientation mapof Al-4% Cu-xCr_2O_3 alloy from optical images (a) 0, (b) 0.75, (c) 1.0 (d) 1.25 (e) 1.5 (f) 1.75 (g) 2.0 (h) 2.25

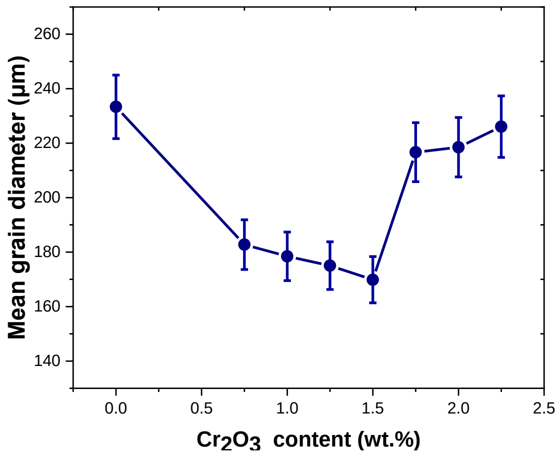

Figure 6. Mean grain diameter of Al-4%Cu-xCr_2O_3 alloys

3.2. SEM microstructural analysis

The SEM, combined with EDS, was used to analyse the formation of intermetallic particles dispersed throughout the microstructure. SEM analysis further provided detailed insights into the dispersion characteristics of Cr_2O_3 particles within the Al-Cu alloy matrix. Figs 7a and 8a illustrate the SEM micrograph of the Al-4%Cu alloy and the corresponding EDS spectrum, respectively. The micrograph reveals that the Al_2Cu intermetallic are coarsely distributed throughout the structures. The microstructure of the base alloy primarily consists of α-Al phase regions, representing aluminium-rich areas interspersed with distinct micro-constituents within the interdendritic regions. The morphology includes α-Al grains and elongated θ-Al_2Cu boundaries, appearing as a dark grey phase with fine, white dotted boundaries, formed via solid-state dissolution of Cu within the Al-matrix. Fig 8a reveals elements like Mg, C, Ti, Fe, and Si in the EDS spectrum, likely formed through the process conditions that produced Al-4%Cu alloy [12]

The presence of finely dispersed particles in the intergranular regions of Al-4%-xCr2O3 alloys were revealed in Figs 7b-h reveal. The SEM-EDS microstructures of the Al-4%Cu alloy with varying Cr_2O_3 contents are shown in Figs 7(b-h) and 8(b-h), respectively. These microstructures revealed a gradual disappearance of the elongated grain boundaries when concentration of Cr_2O_3 increases from 0.75 to 2.25 wt%., indicating coarse primary Al_2Cu particles. The addition of Cr_2O_3 refines the coarse primary Al_2Cu particles in the base alloy's (Al-4%Cu) microstructure, and these notable effects have improved an alloy's mechanical properties under strain [42]. With the addition of Cr_2O_3, fine precipitates of the secondary θ-(Al_2Cu) phase and the β-phase $(AlCr)_2O$ are formed. According to Ramalingam et al [43] chromium (Cr) significantly influences the solidification process by initiating complex heat transfer interactions in both the liquid and solid phases. Chromium accumulation at the liquid-solid interface plays a critical role in refining the dendritic structure of the alloy by promoting constitutional supercooling. This process also enhances undercooling, which, in turn, encourages nucleation and leads to a finer microstructure. As a result, the addition of Cr_2O_3 effectively contributes to the refinement of the dendritic structure in Al-

4%Cu alloys. This is consistent with findings that chromium refines the grain structure in other alloy systems [29,44]. The SEM microstructures show noticeable variations with increasing Cr_2O_3 content, and these morphological differences are corroborated by EDS analysis, which reveals variable elemental intensities in the alloys, confirming the presence of intermetallic compounds.

The EDS analysis (Fig. 8b-h) confirms that the chemical reactions between Cr_2O_3 and the base alloy have been completed, as evidenced by the observed elemental intensities. These intensities indicate the formation of Al_2Cu and $(AlCr)_2O$, with other elements present in alignment with the data shown in Table 2. SEM images of the Al-4%Cu alloy with Cr_2O_3 content ranging from 0.75 to 1.5 wt% reveal a microstructure featuring uniformly distributed dark grey particles. As the Cr_2O_3 content increases from 1.75 to 2.25 wt.%, the dark phase transitions to a light grey phase, suggesting a denser and more non-porous structure [12,22]. The EDS results further confirm chemical composition of the alloys, confirming the presence of aluminium (Al), copper (Cu), and chromium oxide (Cr_2O_3) as primary constituents. Additionally, minor concentrations of carbon (C), silicon (Si), iron (Fe), and magnesium (Mg) were detected as impurities or residual elements.

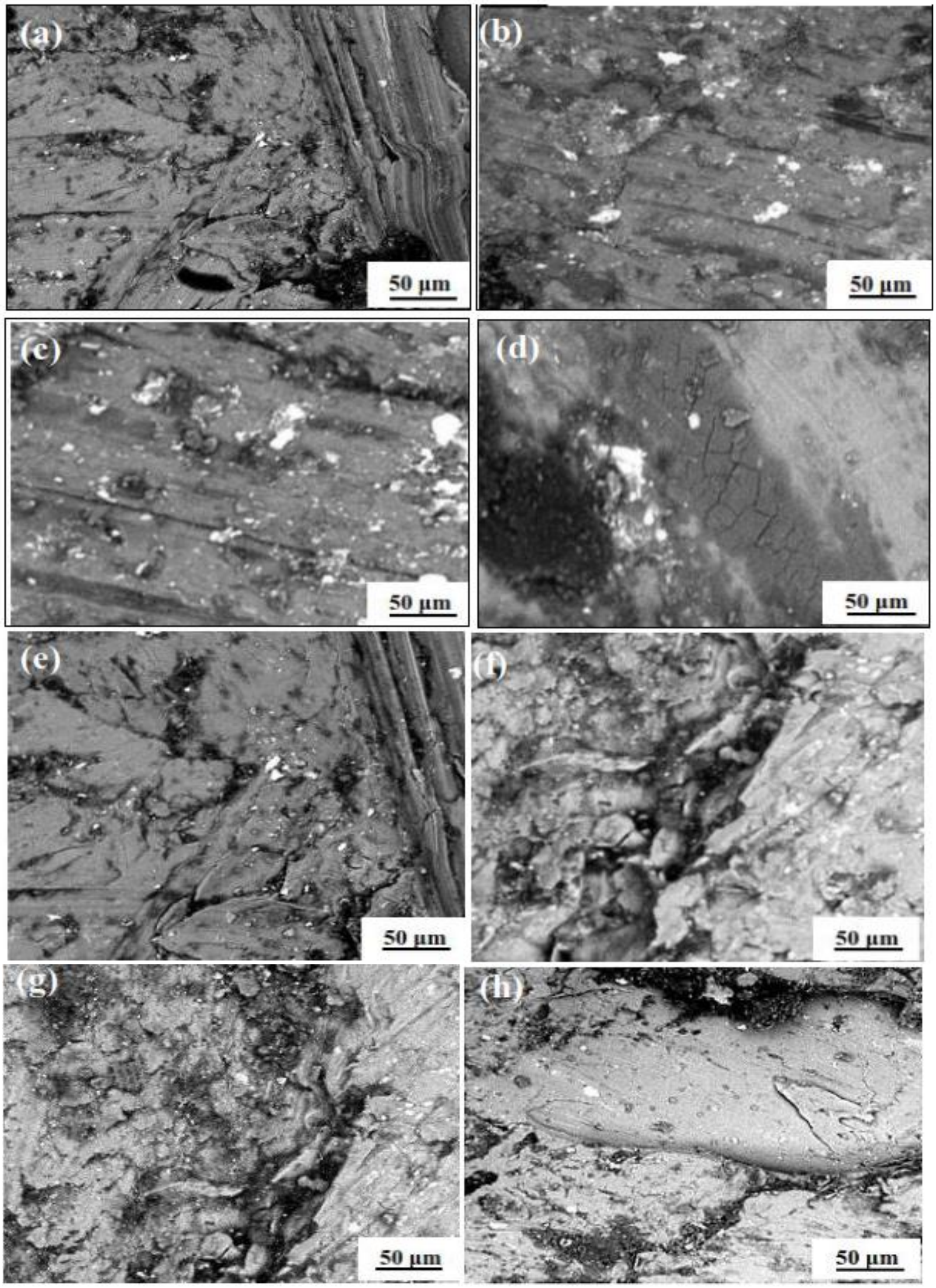

Figure 7. SEM images of Al-4%Cu-xCr_2O_3 alloys at (a) 0%, (b) 0.75%, (c) 1.0%, (d) 1.25% (e) 1.5% (f) 1.75% (g) 2.0% (h) 2.25%

  - Volume 20, Number 3 (ISSN 1995-6665)

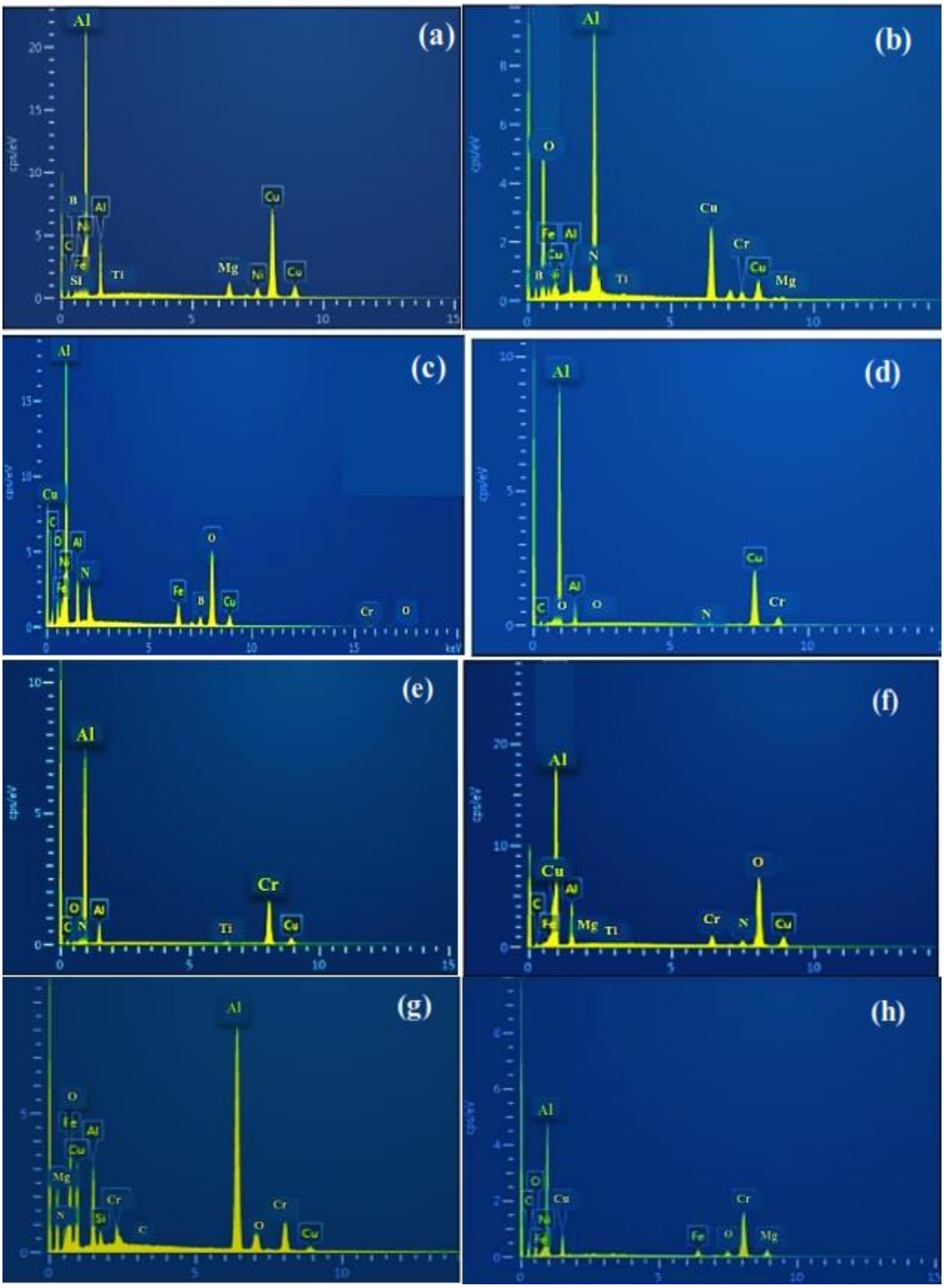

Figure 8. The corresponding EDS of Al-4%Cu-xCr_2O_3 alloys at (a) 0%, (b) 0.75%, (c) 1.0%, (d) 1.25% (e) 1.5% (f) 1.75% (g) 2.0% (h) 2.25%

3.3. Mechanical properties

3.3.1. Tensile characteristics

Figs. 9 and 12 present the mechanical properties of the base Al-4%Cu alloy and the Al-4%Cu alloy with different Cr_2O_3 concentrations. Research indicates that variations in the mechanical properties of aluminium and its alloys are predominantly influenced by phase transformations and microstructural evolution, which play a crucial role in determining the material's overall performance [45,46]. The formation of intermediate phases resulting from the addition of alloying elements is a well-established mechanism for enhancing the strength of alloys, as these phases contribute to grain refinement, precipitation strengthening, and overall microstructural stability [29,42,45,46].

The tensile properties, including ultimate tensile strength, yield strength, and ductility, of Al-4%Cu alloy modified with varying Cr_2O_3 contents in the as-cast condition are shown in Figs. 9(b–c). The corresponding engineering stress-strain curve, which provides insights into the material's deformation behaviour, is presented in Fig. 9(a). The stress-strain curves for Al-4%Cu-xCr_2O_3 alloys exhibit a continuous trend, with stress increasing as strain increases. Notably, Cr_2O_3-doped Al-4%Cu alloys show a significant 67% improvement in tensile properties compared to the base alloy. This enhancement is attributed to Cr_2O_3's effectiveness in refining the coarse dendritic structure of the base alloy. As shown in Figs. 9(a–c), the tensile strength parameters of the developed alloys improve with increasing Cr_2O_3 content. The strength and ductility values increase progressively with the amount of alloying element added, reaching maximum values at 2.25 wt% Cr_2O_3: ultimate tensile strength (UTS) of 362 MPa, yield strength of 199 MPa, and ductility of 13.5%. The refinement of Al grains, as observed in Figure 3, was facilitated by adding of Cr_2O_3 particles into the Al-4%Cu alloy. Material strengthening in metals can take place through three mechanisms: grain refinement, dislocation strengthening, and the Orowan mechanism [38,47]. The mechanism of grain refinement strengthening involves grain boundaries acting as obstacles to dislocation movement. The addition of Cr_2O_3 particles to aluminium alloys promotes this effect by controlling grain size and, consequently, increasing the grain boundary area. This increased grain boundary area then restricts dislocation propagation, resulting in higher strength [28]. In comparison, the Al-4%Cu alloy without Cr_2O_3 exhibits tensile properties of 170 MPa for ultimate tensile strength (UTS), 140 MPa for yield strength, and 10% ductility. However, the incorporation of Cr_2O_3 particles results in a significant enhancement in these properties. The Cr_2O_3-doped Al-4%Cu alloy demonstrates improved strength and ductility, highlighting the beneficial effect of Cr_2O_3 addition. No significant casting defects such as porosity, shrinkage cavities, or inclusions were observed in the machined samples used for mechanical properties test. The consistency observed in the mechanical properties results can be attributed to the vigorous stirring of Cr_2O_3 particles in the molten metal, which ensured a homogeneous dispersion within the aluminium matrix. Furthermore, the use of a steel mould contributed to minimizing casting defects, thereby enhancing the overall quality of the cast samples.

From the observed results, the improvement in tensile strength can be correlated with microstructural refinement, specifically the reduction in Secondary Dendrite Arm Spacing (SDAS), using the Hall–Petch equation. The Hall–Petch equation (Eq. 1) describes the relationship between the strength of the developed alloy and its microstructural features, particularly the grain size [52]:

$$\sigma_y = \sigma_0 + kd^{-\frac{1}{2}} \quad (1)$$

Where σ_y is the strength, σ_0 is the lattice friction stress, k is the hall patch slope which is constant.

By substituting the 51% reduction in SDAS into the Hall–Petch equation, a predicted strength increase of approximately 43% is obtained due to grain refinement. The experimentally observed 53% increase in tensile strength slightly exceeds this prediction, which can be attributed to additional strengthening mechanisms, such as the formation of Cr_2O_3-induced secondary phase particles and improved load transfer. The discrepancy is also influenced by factors like microstructural homogeneity and dislocation-particle interactions. Therefore, the Hall–Petch relationship strongly supports the microstructural origin of the strength gains observed.

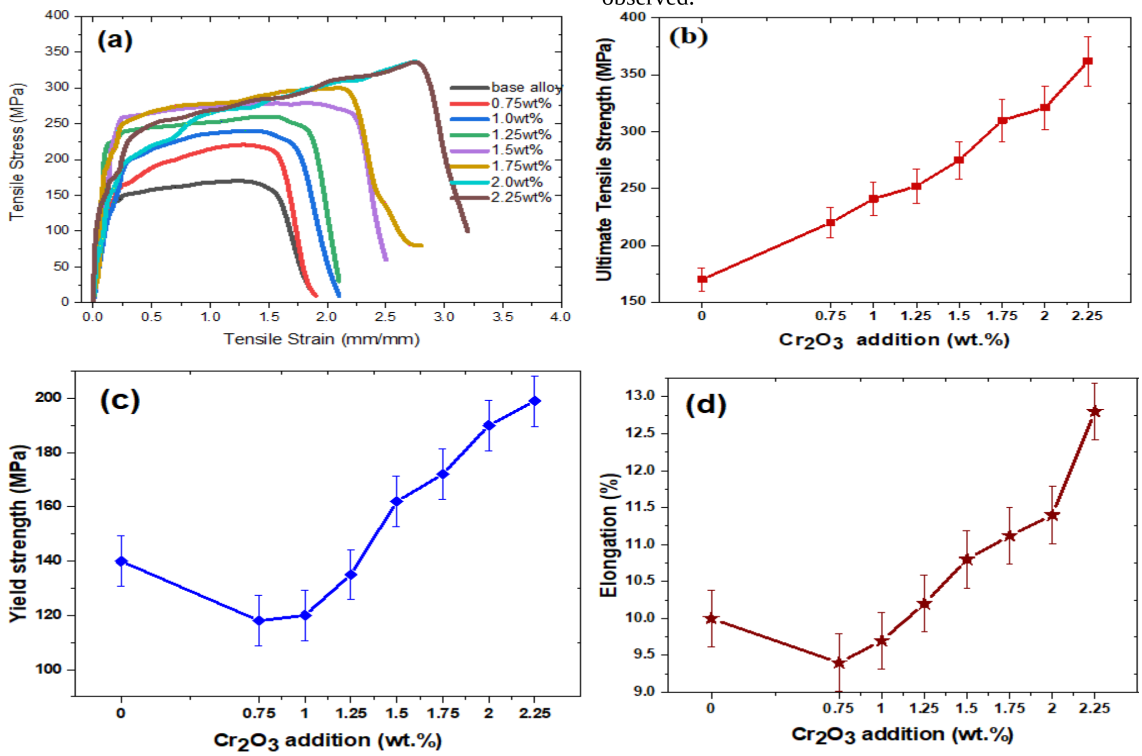

Figure 9. The tensile properties of the developed alloys (a) Tensile stress-strain curve (b) ultimate tensile strength (c) yield strength (d) percentage elongation (ductility)

3.3.2. Fractography

The fracture surface behaviour of the alloys under tensile load was analysed using a scanning electron microscope (SEM). Figs 10 and 11 show the SEM images and three-dimensional (3D) views generated by ImageJ software, illustrating the tensile fracture surfaces of Al-4%Cu-xCr_2O_3 alloys. The SEM images reveal distinct equiaxed pits, indicating localized deformation within the alloy and confirming a mixed brittle-ductile fracture mode. The brittle fracture, ductile fracture and its combination (brittle-ductile fractures), demonstrate the alloy's response to tensile stress. Fig 10a displays the fracture surface of the base alloy, which reveals a coarse quasi-cleavage plane randomly dispersed across the fracture cross-section, with a few torn ridges that suggest is a brittle fracture mode. According to literature findings [42], the coarse structure of the α-Al dendrites cannot strongly impede crack propagation. The torn ridges in Fig 10a are not obvious, and the presence of porosity and cracks given by the cleavage facets indicates poor plasticity in the alloy [22]. In Figs 10b-d, representing the Al-4%Cu alloy with 0.75-1.25 wt% Cr_2O_3, the fracture surface shows primary dimples along with cracks and cleavage facets. The presence of these dimples, is an indication that a ductile fracture mode occurs with alloys, suggesting that alloying with 0.75-1.25 wt% Cr_2O_3 enables the alloy to undergo significant plastic deformation prior to fracture. Dimples are characteristics of plastic deformation as posited by Vignesh et al. [48]. The coarse quasi-cleavage plane in these alloys are reduced, while the tearing ridges increase in size, further emphasizing a mixed-mode fracture but with a predominant ductile behaviour. Figs. 10e-h, where the Al-4%Cu alloy contains higher Cr_2O_3 particle concentrations (1.5-2.25 wt.%), the fracture surfaces revealed are characterized by larger cracks and distinct plastic deformation zones. These plastic deformation zones indicates that the alloys underwent significant stretching and deformation before failure take place. This behaviour reflects an enhanced toughness and ductility recorded within Cr_2O_3 concentration range. The fracture characteristics demonstrated mixed ductile and brittle fracture modes, which is similar to those seen in Figs 10b-d, however, in Fig 10e-h, the regions of tearing ridges, cracks, and cleavage planes are more prominent and widely distributed across the fracture surface. The evolution of fracture behaviour in these alloys can be attributed to Cr_2O_3 addition, which promotes new phase formation and reinforces the interaction between grains and grain boundaries (as shown in Figure 3). This transformation process facilitates tearing during the tensile process [22]. Kamali et al. [3] observed that coarse θ-phases along grain boundaries in an alloy's as-cast microstructure can increase susceptibility to cracking under lower stresses and strains, leading to premature failure, in contrast to finer, metastable phases that improve fracture resistance. This aligns with the findings here, where Cr_2O_3 addition effectively prevents early-stage cracking and enhances tensile properties.

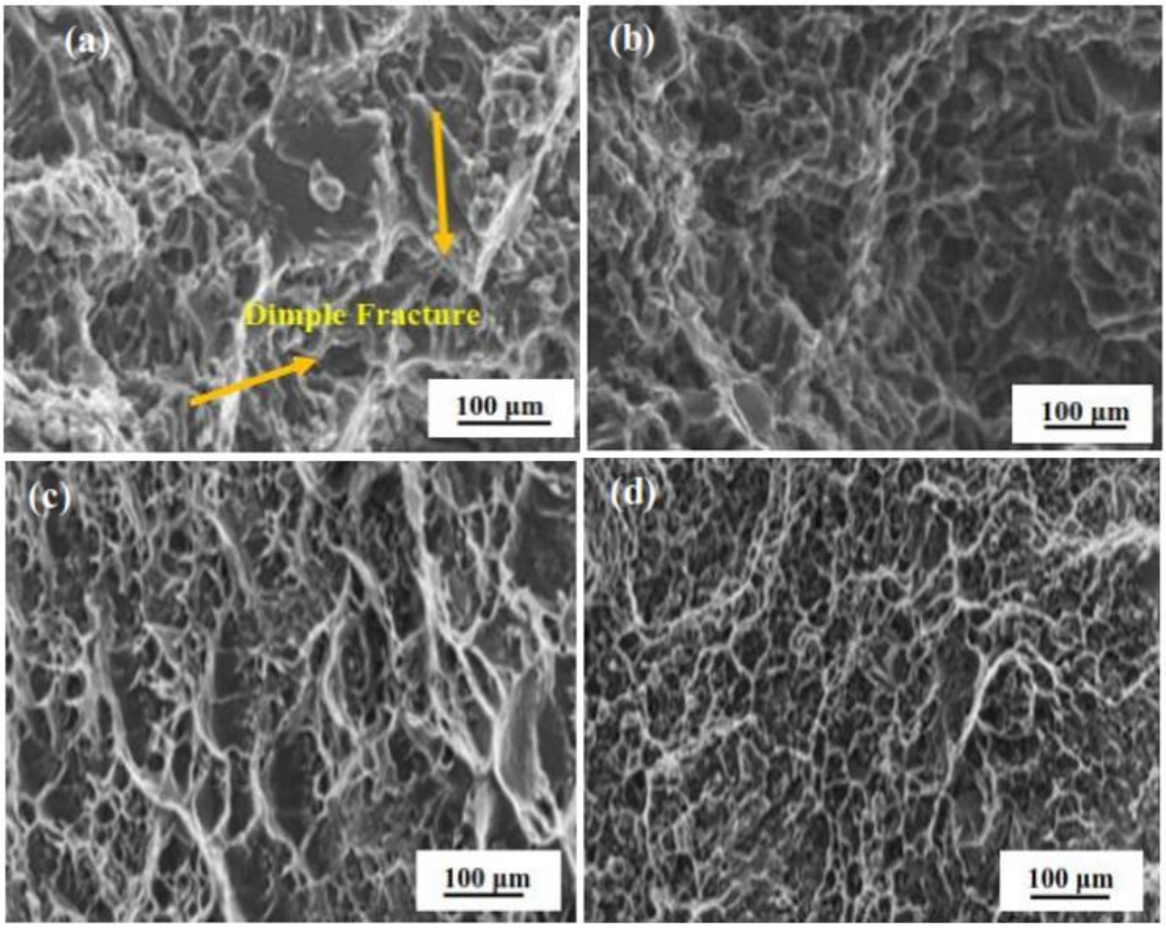

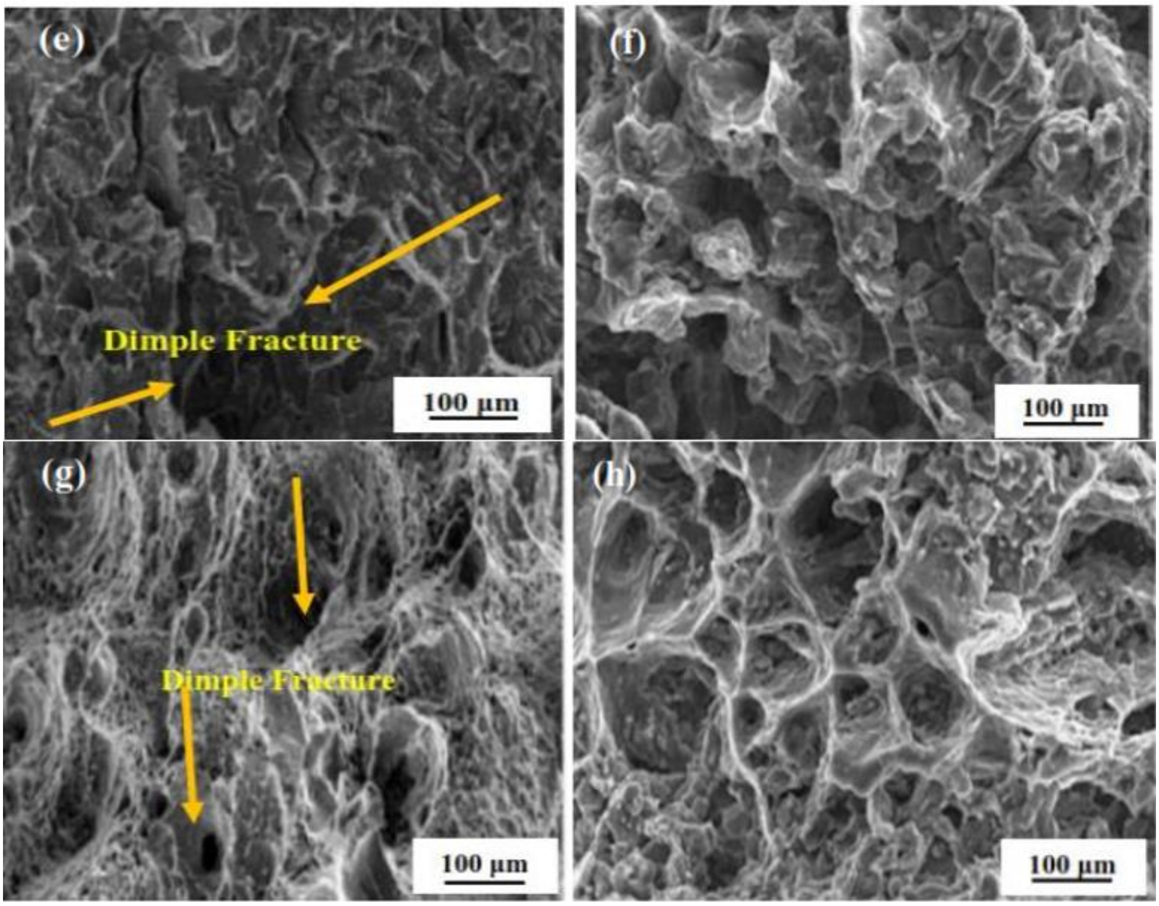

Figure 10. SEM morphologies of the fractured surface of (a) 0 (b) 0.75, (c) 1.0 (d) 1.25 (e) 1.5 (f) 1.75 (g) 2.0% (h) 2.25 wt% of Al-4%Cu-xCr_2O_3 alloys after tensile test

Table 4. Quantitative fracture dimple data.

Sample	Count	Total Area	Average Size(µm)	% Area	Circularity	Feret (µm)	MinFeret	Fracture Behaviour
Al-4Cu	191	5560	29.11	3.72	0.777	7.949	3.901	Predominantly brittle
Al-4Cu + 0.75wt%Cr_2O_3	225	7687	34.164	5.232	0.768	8.737	4.274	Mixed-mode, semi-brittle
Al-4Cu + 1wt%Cr_2O_3	219	4187	19.119	2.892	0.803	6.479	3.247	Mixed-mode, semi-brittle
Al-4Cu + 1.25wt%Cr_2O_3	357	7472	20.93	5.098	0.818	6.812	3.541	Mixed-mode, semi-brittle
Al-4Cu + 1.5wt%Cr_2O_3	439	16739	38.13	10.828	0.77	8.642	4.334	Transitional ductile behaviour
Al-4Cu + 1.75wt%Cr_2O_3	243	7705	31.708	4.824	0.776	8.176	3.855	Abrupt drop in plasticity
Al-4Cu + 2wt%Cr_2O_3	241	62360	258.755	44.993	0.85	7.846	4.054	Most ductile response
Al-4Cu + 2.25wt%Cr_2O_3	271	57904	213.668	40.365	0.829	7.849	3.869	Slight reduction in toughness

Dimples observed on fracture surfaces offer valuable insights into fracture mechanisms and material ductility. SEM analysis of Al-4Cu alloys with varying Cr_2O_3 concentrations reveals how dimple morphology evolves with particle reinforcement. Key parameters—dimple count, average size, %area, circularity, Feret diameter, and MinFeret—were used to assess Cr_2O_3 dispersion efficiency and its impact on fracture behaviour, as summarized in Table 4. The %area of dimples increases significantly with Cr_2O_3 addition, peaking at 44.99% at 2 wt%, indicating enhanced ductility through improved energy absorption and plastic deformation. The sharp rise from 1.5 wt% to 2 wt% suggests a critical threshold where particle distribution promotes void coalescence and crack blunting. However, at 2.25 wt%, a slight decline in %area (40.37%) may indicate particle agglomeration or saturation effects. Although the highest dimple count (439) occurs at 1.5 wt%, the associated low %area (10.83%) suggests clustering and non-uniform deformation. Dimple size follows a similar trend, with the largest average size (258.76 µm²) observed at 2 wt%, reflecting efficient void growth. Lower dimple sizes at 0.75–1.5 wt% indicate reduced void formation, characteristic of semi-brittle or brittle fracture. Larger dimples typically correspond to stable void growth, whereas smaller ones reflect rapid crack propagation. Circularity values support this: 2 wt% (0.85) and 2.25 wt% (0.829) exhibit well-rounded dimples, indicative of uniform ductile fracture. In contrast, lower circularity (e.g., 0.768 at 0.75 wt%) suggests elongated or irregular dimples linked to mixed-mode failure and stress localization. Feret and MinFeret diameters generally correlate with dimple size and distribution. Notably, 1.5 wt% and 0.75 wt% Cr_2O_3 display higher Feret values (>8.6 µm), likely due to elongated or coalesced dimples formed under tensile loading.

The 3D images of the fractured surfaces (Fig. 11) provide valuable insights into the depth and size of the pits formed on the samples. A comparative analysis reveals that the base alloy (Fig. 11a) exhibited relatively smaller pits and shallower depths, indicating a more uniform and less pronounced deformation. In contrast, alloys containing Cr_2O_3 particles displayed more prominent pit formations, with increasing severity corresponding to higher Cr_2O_3 content. Specifically, alloys with Cr_2O_3 content in the range of 1.5–2.25 wt% exhibited significantly larger and deeper pits compared to those with lower concentrations (0.75–1.25 wt%). This trend suggests that the incorporation of Cr_2O_3 particles plays a crucial role in modifying the fracture behavior of the alloy. The observed increase in pit depth and size aligns with the improved mechanical properties, such as ultimate tensile strength (UTS), yield strength, and percentage elongation, as previously presented in Fig. 9. The progressive enhancement in mechanical properties implies that Cr_2O_3 particles contribute to grain refinement and improved load transfer, thereby enhancing the alloy's ductility and strength. Furthermore, the increased roughness and deformation features observed in the 3D images may indicate enhanced energy absorption during fracture, which correlates with the improved toughness of the alloy. Overall, the 3D analysis reinforces the understanding that Cr_2O_3 particle additions influence the fracture mechanisms of Al-4%Cu alloys, promoting a transition from relatively shallow deformation zones in the base alloy to more complex and pronounced features in reinforced compositions. This underscores the significance of Cr_2O_3 as a reinforcing agent in tailoring the mechanical response of aluminum-copper alloys.

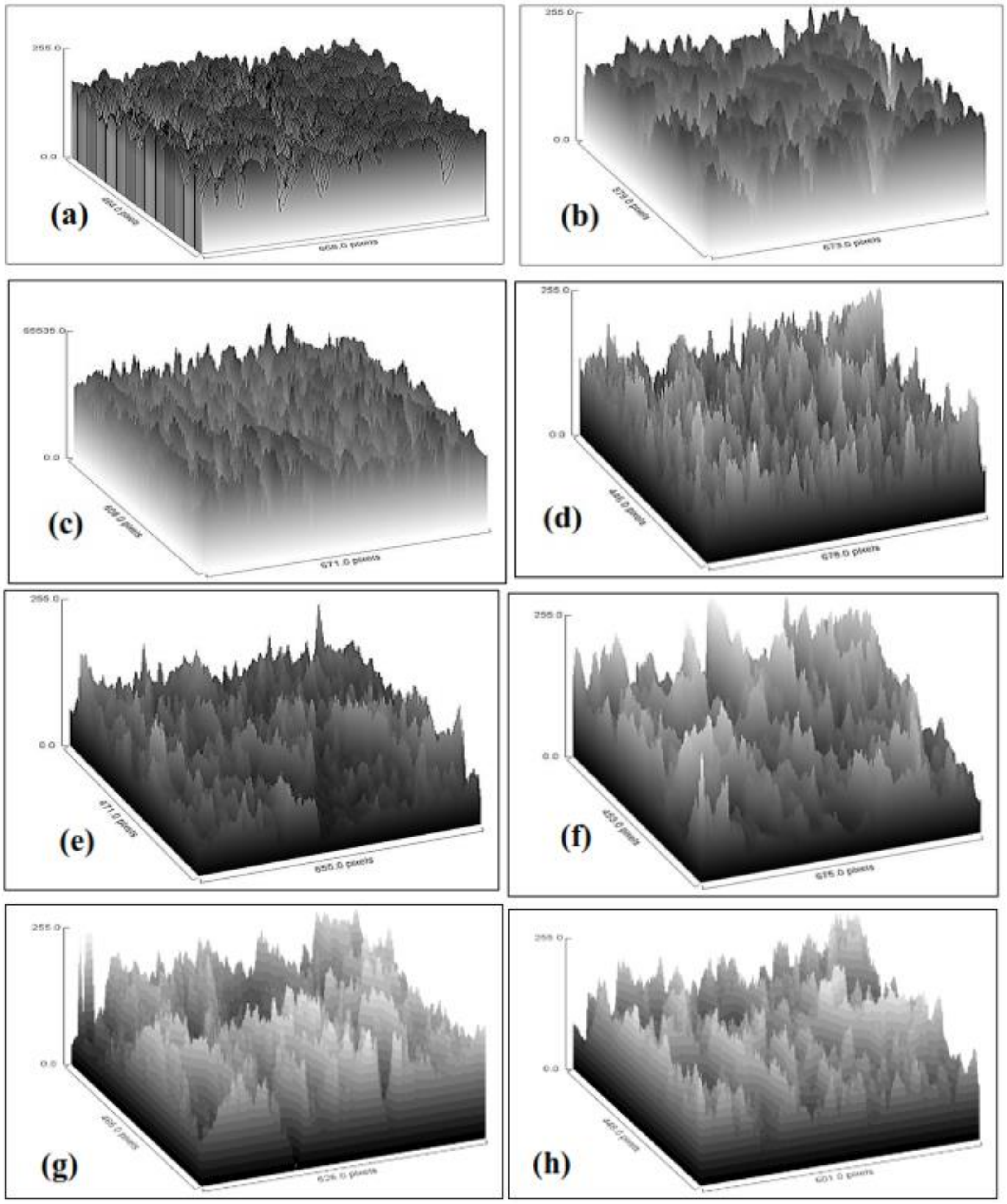

Figure 11. The corresponding 3D views of fractured surface of (a) 0, (b) 0.75, (c) 1.0%, (d) 1.25 (e) 1.5 (f) 1.75 (g) 2.0 (h) 2.25 wt% of Al-4%Cu-xCr_2O_3 alloys

3.3.3. Quantitative fractography–mechanical property correlation

The balance between improvement in strength and the fracture mechanisms is presented in Table 5. The Fractographic Analysis as depicted in Figs 10 and 11 indicates a gradual improvement with increasing Cr_2O_3 content. The SEM fractographs reveal a clear transition in fracture mode with increasing Cr_2O_3 addition in the Al–4Cu alloy. In the unreinforced alloy (0 wt% Cr_2O_3), the fracture surface is characterized mainly by quasi-cleavage/planar regions with limited tearing ridges, indicating relatively rapid crack propagation along coarse dendritic/interdendritic features and reduced plastic energy dissipation, which is consistent with the lowest tensile strength (UTS = 170 MPa). With Cr_2O_3 additions in the low-to-intermediate range (0.75–1.50 wt%), the fracture mechanism progressively shifts toward microvoid-controlled failure, evidenced by fine, uniformly distributed dimples and tearing ridges, reflecting enhanced resistance to crack initiation and propagation; consequently, the tensile strength increases up to 275 MPa while elongation remains stable (≈ 10.8%). At higher additions (≥1.75 wt% up to 2.25 wt%), although extensive dimpling remains evident, the appearance of more pronounced cleavage facets and localized interfacial microcracks suggests an increasing mixed-mode contribution associated with particle/matrix stress concentration or local clustering effects; nevertheless, these conditions correspond to the highest strength levels, reaching UTS = 362 MPa, indicating a predominantly strength-controlled fracture response at elevated Cr_2O_3 content.ImageJ-based dimple metrics (Table 4) correlate strongly with the tensile properties (Table 5), confirming that Cr_2O_3-induced structural modification enhances both strength and deformation capacity. Specifically, UTS shows strong positive correlation with dimple-related ductility indicators, with Pearson correlation coefficients of r ≈ 0.755 (UTS vs. total dimple area), r ≈ 0.745 (UTS vs. % dimple area), and r ≈ 0.708 (UTS vs. average dimple size). This implies that the microstructural refinement and particle strengthening introduced by Cr_2O_3 increase resistance to crack initiation/propagation, allowing higher stress levels to be sustained while promoting distributed microvoid activity at fracture. The sharp improvement in ductile features at higher Cr_2O_3 levels is particularly evident at 2.0 wt%, where the dimple area fraction increases markedly (%Area ≈ 44.99%) with high circularity (0.85), reflecting more stable void growth and enhanced crack blunting.Similarly, elongation increases with increasing dimple-dominated fracture, demonstrating that ductility is governed not merely by void nucleation, but by stable void growth and coalescence over a large fracture area. Pearson correlations show that elongation relates strongly to total dimple area (r ≈ 0.810), % dimple area (r ≈ 0.796), and average dimple size (r ≈ 0.758), validating that alloys exhibiting extensive, rounded dimples undergo greater plastic deformation before final separation. In contrast, dimple count alone is not predictive of tensile behavior (r ≈ 0.237 with UTS), as seen from the 1.50 wt% alloy which exhibits the highest dimple count yet lower dimpled surface coverage than the 2.0–2.25 wt% alloys. Overall, the combined quantitative and qualitative evidence confirms that Cr_2O_3 reinforcement improves the strength–ductility balance primarily through grain refinement and enhanced plastic energy dissipation, shifting fracture from cleavage/porosity-assisted cracking toward a predominantly microvoid-controlled ductile mechanism at optimal compositions.

Table 5. Summary of Fracture Characteristics as a Function of Cr_2O_3 Content

Cr_2O_3 content (wt%)	Elongation (%)	UTS (MPa)	Dominant fracture characteristics	Fracture–property correlation
0.00	10.0	170	Deep, equiaxed dimples; uniform plastic deformation	Ductile fracture with moderate ductility but low strength
0.75	9.4	220	Fine dimples with reduced depth; good matrix continuity	Strength increase with slight reduction in ductility
1.00	9.7	241	Mixed fine dimples and microvoid coalescence	Balanced ductile–mixed fracture; improved load transfer
1.25	10.2	252	Refined dimples; limited particle pull-out	Enhanced strength with recovered ductility
1.50	10.8	275	Uniform fine dimples; strong particle–matrix bonding	Optimal fracture response with high strength and good ductility
1.75	11.12	310	Shallow dimples with initial cleavage facets	Transition from ductile to mixed-mode fracture
2.00	11.4	321	Increased cleavage facets; localized microcracks	Strength-dominated behaviour with reduced plastic deformation
2.25	12.8	362	Cleavage facets, particle agglomeration, interfacial cracking	Mixed brittle–ductile fracture; highest strength with fracture localization

3.3.4. Hardness and ipact strength analysis

The hardness and impact strength results for the Al-4%Cu alloy with varying Cr_2O_3 contents are shown in Fig 12. Both properties follow a similar trend, with the Cr_2O_3-doped alloys demonstrating higher hardness and impact strength than the Cr_2O_3-free alloy. The Al-4%Cu alloy without Cr_2O_3 exhibits lower values, with minimum recorded hardness and impact strength of 75 BHN and 12 J, respectively. The addition of Cr_2O_3 particles significantly improves both hardness (resistance to indentation) and impact strength (energy absorption), with results reflected in higher values compared to the base alloy. The observed enhancement is attributed to dislocations generated during alloy solidification. Studies indicate these dislocations arise due to thermal expansion coefficient differences between the base metal and in-situ formed alloying particles, which contribute to hardening effects and improved toughness in the alloy structure.This phenomenon might be related to particle agglomeration, weakened interfacial bonding, or the formation of brittle intermetallic phases [23,32]. Both properties decreases with increase in Cr_2O_3 content but remain above the base alloy's values. The highest values, 98 BHN and 22 J, were recorded at 0.75 wt% Cr_2O_3, marking an approximate increase of 30.67% in hardness and 83.33% in impact strength compared to the base alloy. This suggests an optimal Cr_2O_3 concentration for maximizing these properties.The noted decrease in hardness and impact strength for higher contents of Cr_2O_3 may be explained on the basis of several microstructural parameters. For higher levels of alloying particle, the particles of Cr_2O_3 are prone to form agglomerations, leading to non-uniform distribution of particles, thus creating the sites for stress concentration. These sites are the prime sites for the generation of cracks even at lower impacts, thus causing lower impact strength []. Further, the high amount of ceramic particles causes weak bonding between the Al-Cu matrix material and the ceramic particles, leading to easy debonding at the interface due to lower stress values [53, 54].

The property trends observed in this study, the increase in strength accompanied by a reduction in toughness with increasing Cr_2O_3 content are consistent with patterns reported for other oxide- and ceramic-reinforced Al–Cu composites. Al_2O_3- and SiC-reinforced Al alloys have widely demonstrated that the incorporation of hard ceramic particles enhances hardness and strength through mechanisms such as load transfer, Orowan strengthening, and dislocation pinning [8, 15]. At the same time, these particles frequently serve as crack initiation sites and reduce the material's ability to undergo plastic deformation, thereby lowering fracture toughness [14, 15, 32]. Our results therefore align with these established trends, suggesting that the strength–toughness trade-off is a general feature of particle-reinforced Al–Cu systems.

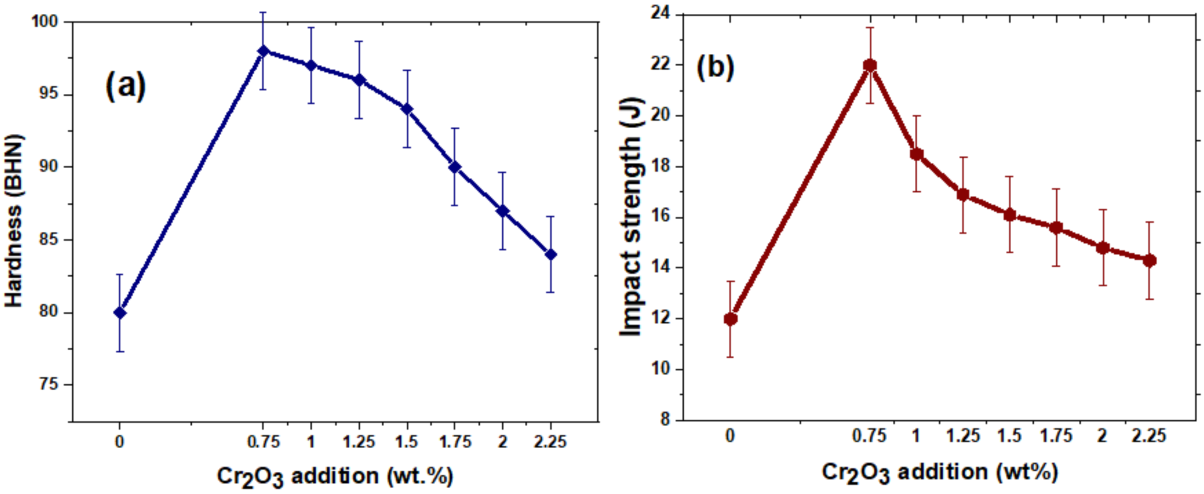

Figure 12. The curve of (a) hardness and (b) impact strength of Al-4%Cu-xCr_2O_3 alloys

4. Conclusions

This study systematically investigated the influence of Cr_2O_3 addition on the microstructural evolution and mechanical properties of Al-4%Cu alloy. The key conclusions derived from the findings are as follows:

1. The addition of Cr_2O_3 particles to Al–4Cu alloy significantly enhanced mechanical performance. The ultimate tensile strength increased from 170 MPa (0 wt% Cr_2O_3) to 362 MPa (2.25 wt% Cr_2O_3), while elongation improved from 10.0% to 12.8%, confirming an overall improvement in the strength–ductility response.
2. For maximum tensile performance and best strength–ductility balance, 2.25 wt% Cr_2O_3 is optimal, whereas 0.75 wt% Cr_2O_3 is optimal for maximizing hardness (98 BHN) and impact energy (22 J).
3. The strengthening improvement is primarily attributed to Cr_2O_3-induced grain refinement and microstructural modification, which reduces dendritic/interdendritic heterogeneity and increases grain boundary barriers to dislocation motion, thereby promoting Hall–Petch-type strengthening and improved structural integrity.
4. Fractography confirms a clear transition in fracture mechanism from quasi-cleavage/porosity-assisted cracking in the base alloy to a predominantly ductile microvoid nucleation–growth–coalescence mechanism at higher Cr_2O_3 contents (particularly 2.0–2.25 wt%), supporting the observed tensile strengthening and improved ductility.
5. The results demonstrate that controlled Cr_2O_3 additions provide a practical route for tailoring Al–Cu cast alloys toward lightweight structural applications where improved tensile strength, deformation capacity, and fracture resistance are required, making the developed composites promising for industrial engineering components.

Competing interest

The authors declare that they have no known financial or competing interests that could have appeared to influence the work reported in this paper.

CRediT authorship contribution statement

E.U. Affiah: Conceptualization, Investigation, Analysis, Writing – draft, review & editing. C.C. Nwaeju-Okechukwu: Analysis, Visualization, Writing – Draft, review & editing. S.O. Okuma: Analysis, Writing – review & editing, F.O. Edoziuno: Analysis, Visualization, Writing – Draft, review & editing.

6.

References

[1] B. Płonka, K. Żyłka, K. Remsak, M. Rajda, J. Zdunek, D. Moszczyńska, Influence of copper content on the structure and properties of aluminium alloys, Archives of Civil and Mechanical Engineering, Vol. 24, 2023, pp. 1–11. https://doi.org/10.1007/s43452-023-00811-7.

[2] E.U. Affiah, C.C. Nwaeju, E.E. Nnuka, Effect of Refractory Oxide (CaO) on the Structure and Mechanical Properties of Al-4%Cu Alloy, International Journal of Scientific Research in Science, Engineering and Technology (IJSRSET) Vol. 1 2015, pp.563–569.

[3] H. Kamali, E. Kamali, M. Emamy, Effects of Zr additions on structure and tensile properties of an Al-4.5Cu-0.3Mg-0.05Ti (wt.%) alloy, China Foundry, Vol. 19, 2022, pp. 9–16. https://doi.org/10.1007/s41230-022-1094-2.

[4] M.-N. Grażyna, K. Gancarczyk, A. Nowotnik, K. Dychtoń, G. Boczkal, Microstructure and Properties of As-Cast and Heat-Treated 2017A Aluminium Alloy Obtained from Scrap Recycling, Materials Vol. 14, No. 1, 2020, pp. 89. https://doi.org/10.3390/ma14010089.

[5] F.C. Campbell, Lightweight materials: understanding the basics, ASM international; 2012.

[6] L. Chen, Y. Wang, X. Hao, X. Zhang, H. Liu, Lightweight refractory high entropy alloy coating by laser cladding on Ti – 6Al – 4V surface, Vacuum , Vol. 183, 2021, pp. 109823. https://doi.org/10.1016/j.vacuum.2020.109823.

[7] B. En, Aluminium and Aluminium Alloys− Chemical Composition and Form of Wrought Products− Part 3: Chemical Composition and Form of Products, BSI; 2007.

[8] E. Affiah, C. Nwaeju, E. Nnuka, The Impact of Refractory Oxides on the Structure and Mechanical Properties of Al-4% Cu Alloy, International Journal of Materials Engineering Vol. 6, 2016, pp.1–7. https://doi.org/10.5923/j.ijme.20160601.01.

[9] M.H. Abdelaziz, E.M. Elgallad, H.W. Doty, F.H. Samuel, Strengthening precipitates and mechanical performance of Al–Si–Cu–Mg cast alloys containing transition elements, Materials Science and Engineering: Vol. 820, 2021, pp. 141497. https://doi.org/10.1016/j.msea.2021.141497.

[10] L. Jiang, T. Langan, T. Wood, P. Sanders, T. Dorin, Isotropy of precipitate distribution in pre-stretched Al-Cu-(Sc)-(Zr) alloys, Scr Mater, Vol. 210, 2022, pp.114452. https://doi.org/10.1016/j.scriptamat.2021.114452.

[11] T. Yang, Y.L. Zhao, Y. Tong, Z.B. Jiao, J. Wei, J.X. Cai, X.D. Han, D. Chen, A. Hu, J.J. Kai, K. Lu, Y. Liu, C.T. Liu, Multicomponent intermetallic nanoparticles and superb mechanical behaviors of complex alloys, Science. Vol. 362, 2018, pp. 933–937. https://doi.org/10.1126/science.aas8815.

[12] R. Su, K. Wang, Y. Yang, Y. Qu, R. Li, Effect of Mg Content on the Microstructure and Corrosion Properties of Al-Cu-Mn Alloy, J Mater Eng Perform Vol. 29, 2020, pp.1622–1629. https://doi.org/10.1007/s11665-020-04684-2.

[13] C. Ren, K. Sun, Y.F. Jia, N.Z. Zhang, Y.D. Jia, G. Wang, Effect of Mo addition on the microstructural evolution and mechanical properties of Fe–Ni–Cr–Mn–Al–Ti high entropy alloys, Materials Science and Engineering: Vol. 864, 2023, pp.144579. https://doi.org/10.1016/j.msea.2023.144579.

[14] H. Wang, H. Zheng, M. Hu, Z. Ma, H. Liu, Synergistic effect of Al_2O_3-decorated reduced graphene oxide on microstructure and mechanical properties of 6061 aluminium alloy, Sci Rep Vol. 14, 2024, pp. 16213. https://doi.org/10.1038/s41598-024-67004-x.

[15] F. Qiu, X. Gao, J. Tang, Y.Y. Gao, S.L. Shu, X. Han, Q. Li, Q.C. Jiang, Microstructures and tensile properties of Al–Cu matrix composites reinforced with nano-sized SiCp fabricated by semisolid stirring process, Metals (Basel) Vol. 7, No. 2. 2017, .pp. 49. https://doi.org/10.3390/met7020049.

[16] R.A. Falcón-Castrejón, J.L. Román-Zubillaga, R. Guardián-Tapia, L. Falcón-Franco, I. Rosales-Cadena, Synthesis and Characterization of Aluminum Alloys with Metal Oxides (CuO_2) Additions as Reinforcementorcement, Materials Sciences and Applications Vol. 14, 2023, pp. 416–425. https://doi.org/10.4236/msa.2023.148027.

[17] R. Kumar, V. Sahni, Effect of Copper and Magnesium Stoichiometric Additions and Thermal Aging on the Mechanical Properties of Cast Aluminium Alloys, Indian J Sci Technol, Vol. 11, 2018, pp. 1–7. https://doi.org/10.17485/ijst/2018/v11i48/138804.

[18] E.R. Wang, X.D. Hui, G.L. Chen, Eutectic Al–Si–Cu–Fe–Mn alloys with enhanced mechanical properties at room and

elevated temperature, Mater Des Vol. 32, 2011, pp.4333–4340. https://doi.org/10.1016/j.matdes.2011.04.005.

[19] M.A. Ibrahim, Y. Sahin, A.Y. Gidado, M.T. Said, Mechanical properties of aluminium matrix composite including SiC/Al2O3 by powder metallurgy-a review, GSJ Vol. 7, No. 3, 2019, pp.23–38.

[20] Z. Chen, P. Chen, C. Ma, Microstructures and mechanical properties of Al-Cu-Mn alloy with La and Sm addition, Rare Metals, Vol. 31, 2012, pp. 332–335. https://doi.org/10.1007/s12598-012-0515-6.

[21] F. Meng, Z. Wang, Y. Zhao, D. Zhang, W. Zhang, Microstructures and Properties Evolution of Al-Cu-Mn Alloy with Addition of Vanadium, Metals (Basel), Vol. 7, 2016, pp.10. https://doi.org/10.3390/met7010010.

[22] S. Wang, G. Meng, M. Song, Effect of Cu Addition on Properties of an Al-La Alloy, Coatings, Vol.13, No.9, 2023, p.1505. https://doi.org/10.3390/coatings13091505.

[23] Q. Zheng, L. Zhang, H. Jiang, J. Zhao, J. He, Effect mechanisms of micro-alloying element La on microstructure and mechanical properties of hypoeutectic Al-Si alloys, J Mater Sci Technol, Vol.47, 2020, . pp142–151. https://doi.org/10.1016/j.jmst.2019.12.021.

[24] C. Tao, X. Yuan, J. Liu, H. Huang, X. Zuo, W. Zheng, Effect of La on hot cracking susceptibility of Al-Cu-Mg alloy, Mater Res Express, Vol. 6, No. 10, 2019, pp 105802. https://doi.org/10.1088/2053-1591/ab41c8.

[25] X. Ding, Y. Lu, J. Wang, X. Li, D. Zhou, Effect of Ce Content on the Microstructure and Mechanical Properties of Al-Cu-Li Alloy, Metals (Basel) Vol. 13, 2023, pp. 253. https://doi.org/10.3390/met13020253.

[26] E. AdabiFiroozjaei, P. Koshy, C.C. Sorrell, Effects of AlPO4 addition on the corrosion resistance of andalusite-based low-cement castables with molten Al-alloy, J Eur Ceram Soc, Vol. 33, 2013, pp.1067–1075. https://doi.org/10.1016/j.jeurceramsoc.2012.11.005.

[27] A.V. Davydiuk, N.E. Kalinina, A.F. Sanin, D.B. Hlushkova, S.V. Demchenko, V.O. Sayenko, Improving the Strength and Corrosion Properties of Aluminium Alloys when Modification with Nanodispersed Compositions, Problems of Atomic Science and Technology, Vol. 5, 2023, pp. 26–29. https://doi.org/10.46813/2023-147-026.

[28] J.B. Agboola, R.H. Khan, S.O. Ubokwe, Effect of Chromium on Grain Refinement of LM11 Aluminium Alloy Sand Castings, FUOYE Journal of Engineering and Technology, Vol. 2, 2017, pp. 59–62. https://doi.org/10.46792/fuoyejet.v2i1.47.

[29] A. Kumar, G. Sharma, C. Sasikumar, S. Shamim, H. Singh, Effect of Cr on Grain Refinement and Mechanical Properties of Al-Si-Mg Alloys, Applied Mechanics and Materials, Vol. 89, 2015, pp. 95–99. https://doi.org/10.4028/www.scientific.net/AMM.789-790.95.

[30] H. Liu, L. Fei, H. Liu, J. Lang, J. Yang, Y. Liu, M. Gao, X. Liu, X. Cheng, M. Wei, Effects of annealing atmosphere on structure, optical and magnetic properties of Zn0.95Cu0.02Cr0.03O diluted magnetic semiconductors, J Alloys Compd, Vol. 587, 2014, pp. 222–226. https://doi.org/10.1016/j.jallcom.2013.10.193.

[31] K. Cui, Y. Zhang, T. Fu, S. Hussain, T. Saad Algarni, J. Wang, X. Zhang, S. Ali, Effects of Cr_2O_3Content on Microstructure and Mechanical Properties of Al2O3 Matrix Composites, Coatings, Vol. 11, 2021, pp. 234. https://doi.org/10.3390/coatings11020234.

[32] A.S. Román, C.M. Méndez, C.A. Gervasi, R.B. Rebak, A.E. Ares, Corrosion Resistance of Aluminum-Copper Alloys with Different Grain Structures, J Mater Eng Perform, Vol. 30, 2021, pp. 131–144. https://doi.org/10.1007/s11665-020-05344-1.

[33] Nwaeju C. C., Odo J. U., Nnuka E. E., Effect of niobium addition on the structure and mechanical properties of aluminum bronze (Cu-10%Al) alloy, Vol 1, No 2, 2015, pp.70-75

[34] M. Li, L. Cai, P. Liu, The effect of Y on microstructure and properties of Al-5wt .% Cu based alloy,Vol. 522, 2012, pp.227–230. https://doi.org/10.4028/www.scientific.net/KEM.522.227.

[35] N.G. Emordi;, I. Sunday;, Onyekpe Basil Obimma, Image J Analysis of Six Different Annealed Temperatures of 0.17% C of HSLA Steels, Word Journal of Engineering and Technology, Vol. 8, 2020, pp.617–629. https://doi.org/10.4236/wjet.2020.84043.

[36] C.C. Nwaeju, F.O. Edoziuno, A.A. Adediran, T.J. Tuaweri, M.S. Kumar, Grain characteristics and mechanical properties of as-cast Cu-10 % Al alloy : Effects of alloying additions, Results in Engineering Vol 12, 2021, pp.100295. https://doi.org/10.1016/j.rineng.2021.100295.

[37] H. Peregrina-Barreto, I.R. Terol-Villalobos, J.J. Rangel-Magdaleno, A.M. Herrera-Navarro, L.A. Morales-Hernández, F. Manríquez-Guerrero, Automatic grain size determination in microstructures using image processing, Measurement, Vol. 46, 2013, pp. 249–258. https://doi.org/10.1016/j.measurement.2012.06.012.

[38] M. Gautam, G. Gautam, A. Mohan, S. Mohan, Enhancing the performance of aluminium by chromium oxide, Mater Res Express, Vol. 6, 2019, pp.126569. https://doi.org/10.1088/2053-1591/ab5818.

[39] F.O. Edoziuno, C.C. Nwaeju, E.E. Nnuka, Morphological evolution and grain size distribution of as-cast and solution treated Cu-Zn-Al alloy, UNIZIK Journal of Engineering and Applied Sciences (UJEAS), Vol.1, No.1, 2023, pp. 23–30

[40] A.B. Andrade, N.S. Ferreira, M.E.G. Valerio, Particle size effects on structural and optical properties of BaF 2 nanoparticles, RSC Adv, Vol. 7, 2017, pp. 26839–26848. https://doi.org/10.1039/C7RA01582H.

[41] H. Zhang, J. He, J. Zhu, J. Sun, X. Zhao, H. Fu, Effect of Mg microalloying on the microstructure and properties of conductive Cu-Ni-Al alloy with ultra-high strength, J Alloys Compd, Vol. 1005, 2024, pp. 176186. https://doi.org/10.1016/j.jallcom.2024.176186.

[42] M. Xu, W. Ding, L. Hu, S. Chen, H. Zhang, H. Yu, W. Zhao, Effects of a novel refiner Al-3Ti-4.35La combined with Sr on microstructure and mechanical properties of as-cast A356 alloy, China Foundry, Vol 21, No. 6, 2024, pp.641-650. https://doi.org/10.1007/s41230-024-3063-4.

[43] V.V. Ramalingam, K.V. Shankar, B. Shankar, R. Abhinandan, A. Dineshkumar, P.A. Adhithyan, K. Velusamy, A. Kapilan, N. Sudheer, Impact of Aging Time on the Metallurgical Properties and Hardness Characteristics of an Al-Si-Mg-Cr Hypoeutectic Alloy Intended for Automotive Applications, Archives of Foundry Engineering, Vol. 24, 2024, pp.137–142. https://doi.org/10.24425/afe.2024.149281.

[44] G. Gumienny, M. Dondzbach, B. Kacprzyk, Effect of Chromium on the Solidification Process and Microstructure of Vermicular Graphite Cast Iron, Archives of Foundry Engineering, Vol.15, 2015, pp 29–34. https://doi.org/10.1515/afe-2015-0054.

[45] Y. Liu, M. Wang, Y. Cao, J. Peng, D. Yang, D. Song, B.O. Okonkwo, J. Wang, E. Han, Revealing the effect of iron content on the microstructure evolution, mechanical properties and corrosion resistance of the A356-T6 aluminum alloys, Journal of Materials Research and Technology, Vol. 33, 2024, pp. 2263–2274. https://doi.org/10.1016/j.jmrt.2024.09.233.

[46] Y. Liu, S. Meng, M. Gao, S. Pan, Y. Fu, R. Guan, Enhanced comprehensive performance via alloying and rheo-diecasting in a semi-solid Al–Si–Fe–Mg–Cu–Sr alloy, Journal of Materials Research and Technology, Vol. 25, 2023, pp. 420–439. https://doi.org/10.1016/j.jmrt.2023.05.222.

[47] N. Srivastava, G.P. Chaudhari, Strengthening in Al alloy nano composites fabricated by ultrasound assisted solidification

technique, Materials Science and Engineering, Vol. 651, 2016, pp. 241–247. https://doi.org/10.1016/j.msea.2015.10.118.

[48] V. Vignesh, B. Sankar, M.C. Chinmay, N. Jeyaprakash, K. V Shankar, G. Krishna, S. Mahesh, K. Harikumar, P. Gopalakrishnan, Impact of Aging Time on the Morphological, Mechanical, and Tribological Behavior of Al-6.6Si-0.2Mg-0.2La Hypoeutectic Alloy, Phys Scr, Vol. 99, 2024, pp.1059a7.https://doi.org/10.1088/1402-4896/ad70f6.

[49] Nyby, C., Guo, X., Saal, J.E. *et al.* Electrochemical metrics for corrosion resistant alloys. *Sci Data, Vol.* **8**, No.1, 2021, pp. 58.. https://doi.org/10.1038/s41597-021-00840-y.

[50] Birks, N., Meier, G. H., & Pettit, F. S. *Introduction to the High-Temperature Oxidation of Metals*. Cambridge University Press; 2006.

[51] Zhang, H., Yu, Z., Wu, R., Ma, X., Feng, X., Ma, Z., Turakhodjaev, N. and Betsofen, S., Evading the strength-corrosion trade-off in high-Li-content Al-Cu-Li alloy through high-pressure heat treatment and artificial aging. *Corrosion Science*, Vol. 246, 2025, pp.112720. https://doi.org/10.1016/j.corsci.2025.112720

[52] Yan, K., Huang, W., Zuo, Z., Liu, J., Ren, P., Hu, D. and Zhao, C., Evaluation of the partitioned mechanical properties and the hall-petch relationship of cast aluminum alloy cylinder head. In *MATEC web of conferences*, Vol. 355, 2022, pp. 01003 https://doi.org/10.1051/matecconf/202235501003

[53] S. Srivastava, Mechanical and water absorption characterization of rice husk and coconut coir reinforced biochar composites, Int. J. Polym. Anal. Charact., Vol. 29, No. 6 2024, pp. 398–409.https://doi.org/10.1080/1023666X.2024.2375254

[54] S. Srivastava, Investigation of mechanical and water absorption characterization of chitosan and rice bran reinforced biochar-based composites, Iran. Polym. J. Vol. 34, No 7, 2025, pp. 1029–1038. https://doi.org/10.1007/s13726-024-01431-5